Int. J. Electrochem. Sci., 11 **(2016)** 9340 – 9354, doi: 10.20964/2016.11.60

International Journal of ELECTROCHEMICAL SCIENCE
www.electrochemsci.org

Analysis of Electrochemical Hydrogen Permeation through AISI Stainless and Welding Zones for Hydrogen Service

M. Miranda[1], *B. Campillo*[2], *Julio C. Villalobos, J. Colín*[3], *A. Torres-_Islas*[3], *A. Molina*[1], *S. Serna*[1,*]

[1]Centro de Investigación en Ingeniería y Ciencias Aplicadas – (IICBA), Universidad Autónoma del Estado de Morelos, Av. Universidad 1001, 62209 Cuernavaca, Morelos, Mexico, [2]ICF- FQ UNAM, Av. Universidad s/n Col Chamilpa Cuernavaca, Morelos, México, [3]Facultad de Ciencias Químicas e Ingeniería, P. A. Ingeniería Mecánica, Universidad Autónoma del Estado de Morelos, Av. Universidad 1001, 62209 Cuernavaca, Morelos, México
[*]E-mail: aserna@uaem.mx

Received: 8 August 2016 / *Accepted:* 15 September 2016 / *Published:* 10 October 2016

Stainless Steel proved to be very valuable material for humankind modern technology, today concepts like global warming and sustainable alternate technologies have become important concepts to actual human survival. One of the most sounded, reliable and ecofriendly technology was developed around a simple element, named hydrogen. Hydrogen economy, that is Fuel Cells System Economy, needs the use of hydrogen embrittlement resistance materials for housings, valves and springs, etc. From the vast possible materials two modern austenitic alloy AISI grades 304 and 316 types, were studied by high fugacity hydrogen conditions (electrochemical hydrogen charge) in smooth and welded specimens by the hydrogen permeability technique developed by Devanathan and Starchursky. Stainless steels are well known to be more resistance to hydrogen embrittlement effects, than ferritic steels. Recently austenitic 316 alloy has been proposed to fulfill hydrogen economy demands. However, more data are needed in order to identify hydrogen embrittlement mechanisms for this alloy and its welding condition. Austenitic alloy 304 was studied comparing smooth and TG welding conditions as well. The results reveal that alloy 316 has good performance under hydrogen embrittlement conditions its chemical composition modified with molybdenum infers different hydrogen embrittlement mechanisms related to austenitic alloy 304. The different carbides formed in both austenitic alloys give substantial differences in their microstructures that finally result in different interactions with hydrogen embrittlement mechanism. A relevant result is that apparently austenitic alloy 304 has more resistance to hydrogen embrittlement, this seems to be by the lack of formation of the chi phase that is more likely to be formed in austenitic alloy 316. The TIG welding conditions for both stainless steels move the differences apart more between both stainless steel microstructures. Both stainless steels could be more susceptible to HE by their related mechanisms than in their respective HAZ and WZ.

Keywords: Hydrogen service, electrochemical hydrogen permeation, stainless steel, TIG welding, welding zones.

1. INTRODUCTION

There is no doubt about the importance of Stainless Steels (SSs) in our modern civilization. For steel to be called "stainless steel", chromium must be at least about 11 wt. %, at this Cr a self-healing chromium oxide film can form in moderately harsh environments. Nevertheless, to prevent pitting and rusting in more aggressive media higher Cr contents must be add-on. The Fe–Cr system is the basis, contemporary stainless steels but, in addition to Cr, a host of supplementary alloying elements could be present to enhances specific properties. There is six principal kind of SSs named, ferritic, austenitic, martensitic, (duplex, precipitation hardening and (Mn-N substituted. These groups of stainless steels have miscellaneous properties, and they have been broadly and well recognized in the existing literature [1].

On the other hand, hydrogen is recognized as a medium for energy storage for static and portable power generation. Fluid system components for hydrogen delivery, containment and refueling that are made of austenitic SS must hold mechanical properties when they are interacting with hydrogen [2]. AISI 316 stainless steel represents particularly attractive candidates for components in hydrogen service [3]. AISI 304 stainless steel was used for comparison, furthermore, type 304 has also been used in high fugacity conditions as encountered in sour service for the oil and gas industry [4], in which hydrogen is a by-product of SSs corrosion in contact with the environment.

300 grade series AISI Austenitic comprise chromium and nickel in addition Type 316 is a chromium nickel stainless steel (SS) containing molybdenum. Molybdenum surplus n increases its pitting and general corrosion resistance [5].

Is generally considered that the austenitic class 300stainless steels has good weldability by the usual fusion resistance techniques. Different compositions among 304 and 316 types (304 contains 18% chromium and 8% nickel while 316 contains 16% chromium, 10% nickel and 2% molybdenum), seems not generate different welding performance s between them. Alloy type 316 has excellent weldability with and without filler metals, but is well known that heavy welded sections need post-weld annealing for maximum corrosion resistance, this is not required for 316L in which L denotes low Carbon content [6]. To avoid weld "hot cracking special measures has to be taken assuring formation of ferrite in the weld deposit [7].

Certainly, a percentage of SSs components like valves, fittings, and other fluid system components or other machinery parts are used for hydrogen service at elevated temperatures, or simply by welding the SSs. High-temperature exposure, can develop numerous phases that may precipitate in the several classes of stainless steels. The formation of these precipitates began when reheating above 300 °C SSs [8]. This precipitates have deep consequences on their properties and it is not surprising that these precipitates are almost always viewed as being deleterious and some like the $M_{23}C_6$ carbide, can be common to all SSs classes.

Even though, austenitic SSs due their high activation enthalpy for hydrogen mobility have higher resistance to hydrogen embroilment (HE) 0.52–0.57 eV [9]) than nickel and alpha-iron, in atmospheres where the pressure of gaseous hydrogen is high or in cathodic charging, austenitic SS will still suffer HE. Moreover, austenitic SSs by their high content of Cr and Ni, generate a passive layer of Cr_2O_3 that acts as a barrier, reducing the gradient of concentration of hydrogen on the surface of steel.

However, this type of steel has increased susceptibility to HE in the areas of welding (WF and HAZ), caused by a phenomenon of sensitization where a chromium carbides ($Cr_{23}C_6$) precipitation occurs at the grain boundaries [10], generating, a greater number of sites of entrapment, weakening the grain boundaries. There is also a decrease in the content of Cr in the matrix making the SSs more susceptible to intergranular corrosion and HE [11].

Recent publications have settled controversies, such as the foremost mechanism accountable for causing HE. Indeed, several current works have persuasively demonstrated that HELP (hydrogen-enhanced localized plasticity) is the primary mechanism for causing HE in austenitic stainless steels [12-13].

The interaction with hydrogen of SSs depends on the stress-state, but mainly on the different microstructural features present. So, the aim of this work is evaluate hydrogen effects on 304 and 316 SSs, hydrogen diffusion (permeation) experiments were done under high fugacity conditions, while receiving smooth commercially SSs and after autogenously welded membrane samples. Another important issue is that the welding zones tend to have two-phase dendritic microstructures, as a possible result of ferrite-containing welds in AISI 316 and 304 SSs could have made more susceptible to hydrogen-damage mechanisms.

2. EXPERIMENTAL PROCEDURES

2.1 Materials

Two austenitic SSs plates were used for this study, type 316 and type 304, plate dimensions were of 203.2 and 127 mm (8 and 5 inches) length and wide respectively, with thickness of 6.35 mm. (1/4 inch). Chemical composition in weight % was determined by Spark Mass Emission Spectroscopy, the chemical compositions of the two SSs are shown in Table 1.

Table 1. Chemical composition of the two SSs.

Steel	C	Cr	Ni	Mn	Si	S	P	Mo
304	0.08	15.51	7.2	2.0	1.0	0.03	0.04	-
316	0.08	14.99	9.21	2.0	1.0	0.03	0.04	1.86

Apparently, 304 Type do not fulfill Cr standard composition around 18 in wt. % but presents a higher amount of Cr than type 316. The Ni content fulfils standard compositions, and type 316 has about 2 % in wt. of Mo. It could be seen from Table 1 that other elements are present like Mn and Si an important percentage, S and P seem like impurities for both alloys.

Austenitic SSs metallography preparation was made in order to obtain their respectively microstructures by standard methodology that includes, polishing and chemical attack, using the following analytical grade chemical reagents 10 ml HNO_3, 10 ml. $C_2H_4O_2$, 15 ml. de HCl, 2-5 drops of

de glycerol according to ASTM Standard E-407 [14]. SSs microstructures were observed by optical microscopy and SEM (JEOL 6300 operated at 15~20 kV and equipped by an EDX analyzer).

2.2 Welding Procedure

Before welding, the plates were lightly ground using 150-grit flexible abrasive paper and then cleaned with alcohol, in order to weld bead on the plate's surface.

Each austenitic SSs plate was welded by using a TIG (tungsten inert gas) UCC-305 POWER SUPPLY welding machine. This machine uses a permanent thorium-tungsten electrode (diameter 3.2 mm, 60 o vertex angle) and the welding was autogenously made, with a constant distance approximately 4.8 mm arc length and an electrode displacement velocity of 1.9565 x 10-3 m/s. Argon was employed as shielding gas at a flow rate of 5 l/min. A direct current polarity (DCSP) of 220 A was used, and the experiments were made by approximately 35 sec of arcing, so that steady state conditions were achieved and one SS plate (anode) mounted to a water-cooled copper wall.

Single pass welding minimizes the heat treatment effect of subsequent passes, which may obscure fundamental effects. Fusion runs provide weld metal of identical chemistry to the base metal.

2.3 Hydrogen permeability test

Austenitic SS membranes of types 316 and 304 in as received and welding conditions with a superficial area of 15 mm^2 according ASTM Standard G-148 [15] and thickness around

200 to 600 µm. Both sides of SSs membranes were polished up to 2000 grit paper, later, a physical vapor deposition (PVD) of Au/Pd was carried out by the "magnetron sputtering" technique. After that, an electrochemical permeation technique originally developed by Devanathan and Starchursky [16] was used as seen in figure 1 to determine the permeability parameters such as permeability flux, diffusion rate and concentration of hydrogen through the lattice for all SSs membranes from various zones, such as the weld metal, the HAZ and the base metal.

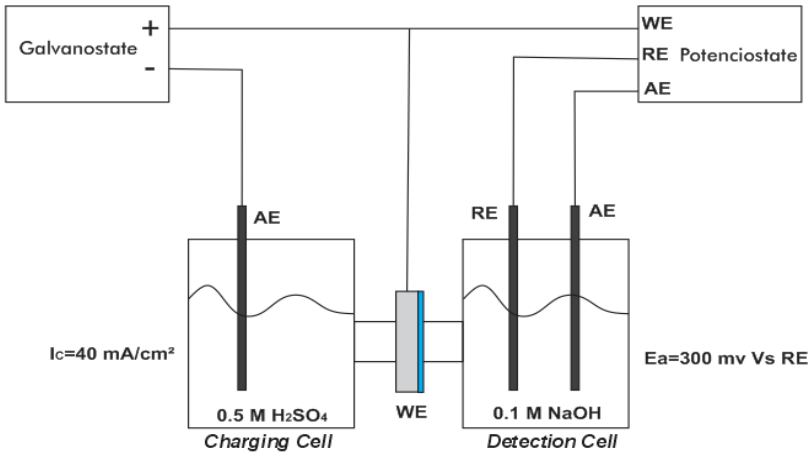

Figure 1. Double electrochemical cell for permeability test.

The experiment consisted of two-component electrochemical cell, separated by the SS steel membrane. The hydrogen charging cell solution was 0.5 M H_2SO_4 + 0.2 g. As_2O_3 with a cathodic polarization current of 40 mA/cm^2, relative to the saturated calomel electrode (SCE). The hydrogen exit cell or detection hydrogen cell was filled with 0.1 M NaOH. The hydrogen permeation current was measured with a membrane oxidation potential of 300 mV vs SCE. The coated with gold-palladium (Au/Pd) SS membranes help minimize the background current density and significant hydrogen permeation current density could be obtained. These helped to prevent non oxidized atoms which were not accounted in the hydrogen permeation current. All the solutions were made from the analytic grade reagents and distilled water, and a platinum wire as an auxiliary electrode. All the tests were performed at room temperature.

Considering a one-dimensional diffusion through a membrane of thickness L, the diffusion coefficient was determined by the permeability transient analysis J(t). The diffusion coefficient can be calculated from equation 1.

3. RESULTS AND DISCUSSION

3.1 Material Characterization

TIG was used for SS plates welding under the conditions mentioned above, having as main advantage the obtaining of more resistant cords, ductile and less sensitive to corrosion, compared to other welding procedures, since the protective gas prevents contact between the environmental oxygen and the welding pool. Subsequently welded SS plates were cut and polished without the superficial and transversal fusion zone. Figure 2 presents a metallography of the macroscopic weld to observe the surface and depth of the weld, showing a good weld penetration depth for steel 304 and 316.

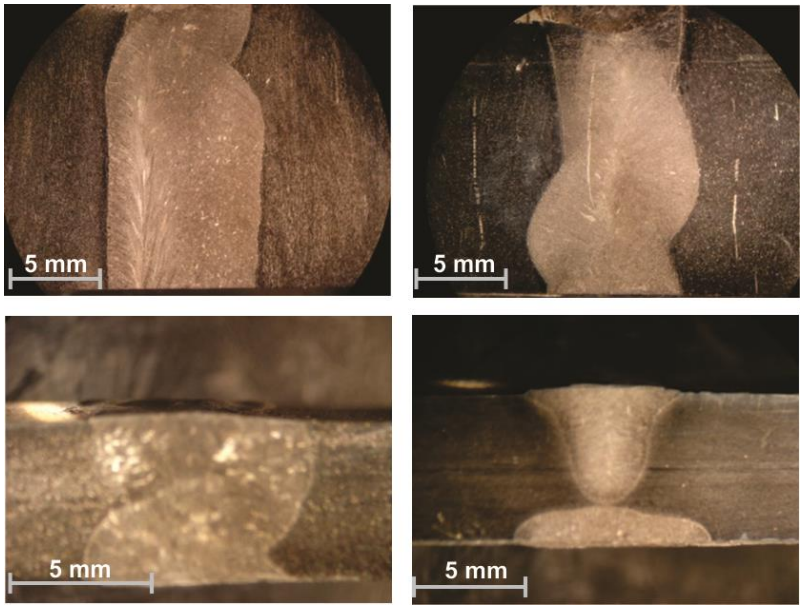

Figure 2. Welding zone stereographic macrograph of the austenitic SS. a) 304 surface, b) 304 cross-section, c) 316 surface and d) 316 cross-section.

The fusion zone (weld metal) microstructure in figure 3 was constituted by slight ferrites (delta-dark etching) in the columnar grain and sub-grain dendritic boundaries in the austenite matrix. The weld metal did not involve twin structure. A magnetic measurement made during the characterization, exposed the delta ferrite content in the weld metal at about 8%. It is well known that, in the weld metal, delta ferrite can overwhelm hot cracking during solidification of austenitic stainless steel welds [17]. Nevertheless, the occurrence of delta ferrite, having an inferior hydrogen solubility and a greater hydrogen diffusivity, may rise the HE susceptibility of the weld. Furthermore, fusion zone residual tensile stresses introduced after welding, can produce harmful effects.

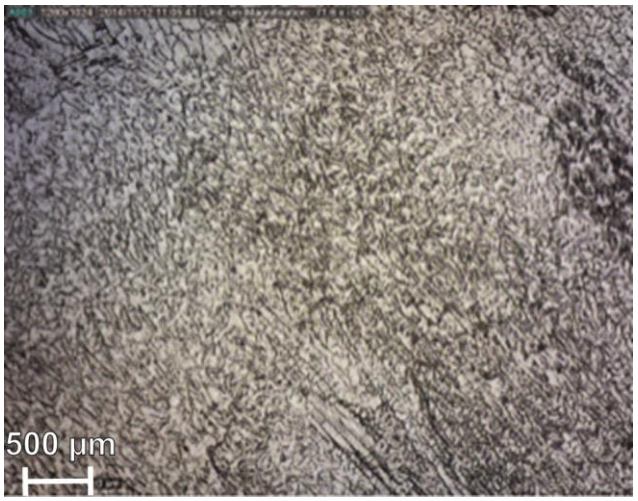

Figure 3. Fusion zone (WZ) solidified in the FA mode.

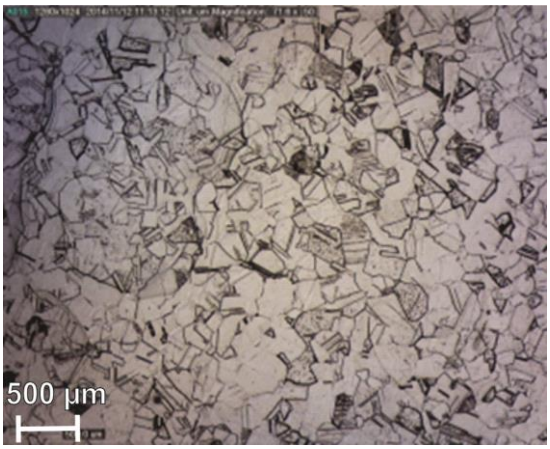

Figure 4. Type 304 and Type 316 base metal microstructure.

The room-temperature microstructure of the fusion zone of austenitic stainless steels is dependent on both the solidification behavior and subsequent solid-state transformations.

There are four solidification and solid-state transformation modes for austenitic stainless steel weldments. Solidifying compositions in FA and F modes pass through the two phase (delta ↔ gamma) area and re-enter the single-phase austenite field, due to the asymmetry of the two-phase field near the

primary ferritic side [18]. Consequently, fully austenitic Type 304 and 316 alloys at room temperature re-enter this two-phase region after AF/FA solidification and undergo fully austenitic structure solid-state transformation, as seen in Figure 3. It was found that the main factor of hot cracking susceptibility is the solidification mode. Thus, guaranteeing an FA or F solidification ensures the best resistance to hot cracking [19].

Figure 4 shows base metal typical microstructure representative of the two type of steels consisting of equiaxial austenite grains with some twins, but no evidence of delta ferrite in the matrix. This microstructure is generated after severely hot rolling in the solution annealed condition and afterwards, cooling of the type 316 and type 304 austenitic plates.

A variety of precipitates may be present in austenitic stainless steels, depending on composition and heat treatment or welding process, since chromium is a strong carbide former. Additions of other carbide formers, including Mo, Nb, and Ti, also promote carbide formation. Other phases can also be formed like nitrides and intermetallic phases.

According to the Fe-Cr diagram [20] for 304 and 316 types due to high Cr (if Cr>20%) availability in both steels, a hard, brittle, low-temperature equilibrium phase, sigma phase is present, with (Fe, Cr) stoichiometry. However, from table 1, we can see that both SSs do not pass 16% Cr, in SSs, an excess of 17% Cr is needed to begin sigma formation, and due to the kinetics of formation of sigma phase, it is quite sluggish and precipitation requires extended time in the temperature range 600 to 800°C. Therefore, it is reasonably to say that sigma is not present in neither of SSs under study. Another harmful phase which hardly can be formed at the present SSs composition is the alpha prime because it precipitates beyond the sigma + α phase field at temperature of 475°C, with Cr contents >40%. The presence of the above precipitates results in severe embrittlement [21]. Nor addition of Ti or Nb strong carbide former was added to either both steels. Thus, presumably any hurtful carbide evolved by these elements cannot be present. There was no presence of N (nitrogen) in both steels, so the epsilon phase could not be formed, in both base plates SSs grades 316 and 304.

Figure 5 presents the interphase between the HAZ and weld metal (dark etched-fusion zone), but no difference could be found between the HAZ and the base metal by optical microscopy, when comparing Figure 4 and 5.

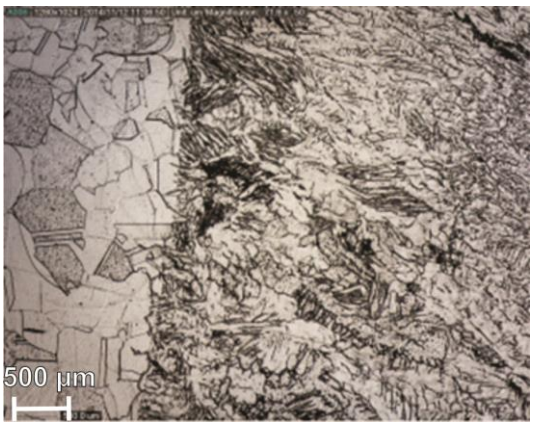

Figure 5. Interphase between the HAZ and weld metal al at 100X obtained by optical microscopy.

Most stainless steels are welded in the solution-annealed or hot-rolled condition, so grain growth is usually restricted. In this interphase, the evolution of many precipitates can be take place due to a supersaturation of C in the HAZ and weld zone, at welding temperatures and with no further uniformly cooling of the weld metal grain boundaries and HAZ. Even though not apparent metallographic ally, it is likely that these precipitates will be present in the HAZ of most austenitic alloys. Their size, distribution, and morphology are dependent on the alloy composition and the HAZ thermal cycle. Carbides and nitrides are the most likely precipitates to form the HAZ.

Although slow cooling from or refrying within the range of 550-800°C leading to a solution carbon rejection, usually as the chromium-rich carbide, $Cr_{23}C_6$, the carbon content is very low (<0.03 wt.%). Welding, in particular, provides these conditions in the heat affected zone (HAZ). Unfortunately, this carbide, which is the most harmful carbide in austenitic SSs, could be formed for type 304 because of its carbon content above 0.03 wt%. In the case of 316 type although it has the same carbon content, 0.08 wt%, the $Cr_{23}C_6$ reaction kinetics can be controlled by the addition of molybdenum [22]. As seen from Table 1 type 316 contains enough Mo to markedly lengthen the sensitization time. Exposure of austenitic steels to air at temperatures greater than 600°C can lead to very high (>1 wt%) nitrogen concentrations under the oxide layer, with coarse Cr_2N (epsilon-phase) matrix precipitation, as well as discontinuous lamellar precipitation at grain boundaries [22]. At last the (FeCrMo) chi intermetallic phase would be present in type 316 because of its Mo content after welding. The chi phase forms earlier than the sigma phase, it transforms to the sigma phase but only upon prolonged ageing [23].

3.2 Hydrogen Diffusion.

For analyzing the current data of the hydrogen permeation experiments correctly, the first stage is to fit experimental results with the appropriate model (initial and boundary conditions). Then use the proper mathematical relations to determine parameters as hydrogen diffusivity and sub-surface hydrogen concentration.

The steady-state flux of hydrogen (J_{SS}, mole H s^{-1} $cm^{-2)}$ through the specimen was measured in terms of steady-state current density ($i\text{-}_{steady}$), and $J_S = i\text{-}_{steady}/nF$, where n is the number of electrons transferred (n=1), and F is Faraday's constant (96,485 C/mol). The permeation flux (mole H s^{-1} cm^{-1}) is defined by $J_S L = i_{steady} L/nF$ in which L is the steel membrane thickness.

In the course of fitting the permeation curves of the experiments, the time of relaxation and then the normalized curve were corrected for (J_S/J_{SS}) and then plotted as illustrated by Figure 6 and 7, for the base, HAZ, welding or fused metal and for simple lattice hydrogen diffusion. The Constant Concentration (CC) model for these experimental data fits well as defined by either the Fourier or Laplace dimensionless equations described elsewhere, [24] and reproduced here by eq. 1.

$$\frac{J_S}{J_{SS}} = 1 + 2\sum_{n=1}^{\infty}(-1)^n \exp\left(-n^2\pi^2\frac{D\times t}{L^2}\right) \qquad \textit{eq. 1}$$

This ratio, between hydrogen permeation transient J_s *and the steady state flux* J_{ss} corresponds to the Fick second law, which depends of the diffusion coefficient D_{app}, calculated by equation 2 and from a membrane of thickness L.

$$D_{app} = L^2/15.3t_b \qquad \textit{eq. 2}$$

where, t_b is the steady state time and L is the membrane thickness (cm). The steady state time could be obtained by the initial hydrogen permeation current transient lineal segment extrapolation when t = 0 [25].

Once the steady state was reached, hydrogen concentration C_0 can be computed in the superficial entrance by the first Fick law, *Jss* and the diffusion coefficient D_{app}. The apparent hydrogen solubility C_0 (mole H cm-$^{3)}$ is determined by equation 3.

$$C_o = \left[\frac{J_{ss} \times L}{F \times D_{app}}\right] \times \left[\frac{M_H \times 10^6}{\rho_{Fe}}\right] \qquad \textit{eq. 3}$$

where L is the membrane thickness, t is the time when the current density corresponds to 10% of the steady state, F is the Faraday constant (96,485 C/mol), M_H molar mass of hydrogen (1g/mol) and ρ_{Fe} is the iron density (7.87 x10^6 g/m^3).

This model, assumes that the sub-surface hydrogen concentration (C_0), is recognized rapidly. Practically, the C_0 value changes to some extent meanwhile the corrosion potential of the steel each the steady-state. This time is always small, related to the experimental time-to-breakthrough for hydrogen permeation. Thus, any error is considered irrelevant.

3.2.1 SS type 304 hydrogen diffusion.

Figure 6, shows the hydrogen permeation transients obtained from different zones of SS 304 named, base metal, HAZ and welding, which correspond to the melted or welded steel zone. Figure 6a corresponds to the first transient and figure 6b show the second transient.

Both graphs in figure 6 illustrate the normalized hydrogen flux variation as a function of the normalized time (Dt/a²). Using the numerical solution for Fick second law (eq. 1), a simple diffusion curve was determined that represents the hydrogen permeation in the SS lattice without the influence of possible defects such as second phase particles, vacancies, grain boundaries and dislocations that could impede the free transit of the hydrogen through the SS crystal net. This curve serves as a base of comparison with respect to the number of hydrogen tramps that the SS could have in the different zones mentioned above.

It was observed that the normalized permeability flux increases rapidly for the HAZ zone reaching the stable state at a time of 0.5. However, for the WZ and Base Metal (BM), it requires more time to reach the stable state (0.8 and 1.16 respectively).

This behavior is similar when the second transient was carried out (figure 6b), but a difference stands out, the times required for the steady state are more prolonged for each analyzed zone. In

addition, the same polarization curve was not reached, this was lightly minor. This clearly denotes the presence of two types of hydrogen traps, reversible and irreversible traps. Once the first transient was made both types of tramps were fulfilled by the SS acquiring its maximum hydrogen saturation when it reaches the stable state. When the cathodic polarization is retired with the acid solution in the charging electrochemical cell, a degassing process takes place, where irreversible tramps with less trapping energies liberate hydrogen thus permitting a major fugacity out of the 304 SS.

When the second cathodic polarization was done, a certain hydrogen quantity remains in steel irreversible traps. This implies a less permeability flux, with the required times growing to achieve the steady state condition. This process will largely depend on the speed of entrapment and deliverance of the traps. There also exist conditions in the exit electrochemical side, this formation of a Cr_2O_3 protective film in the absence of Pd that acts as a hydrogen flux barrier, and could affect stable state hydrogen permeation [26].

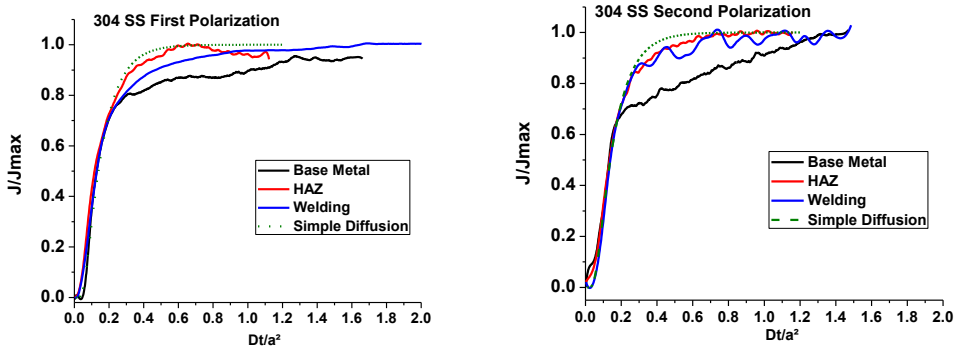

Figure 6. Permeability curves of 304 steel, a) first polarization, b) second polarization.

Once the hydrogen transients are obtained, the parameters of apparent concentration and diffusion velocity for the first and second transient of the SS 304, (see figure 7a and b) were calculated. These graphics indicate that the BM presented a major concentration of hydrogen, 0.35 and 0.2 ppm, for the first and second transient respectively. For the HAZ and WZ this value was near 0.05 ppm for both transients, and much less for the BM. With respect to the hydrogen rate diffusion coefficient the BM presents a value of 5.20×10^{-9} cm²/s, for both transients this value was the same. The diffusion velocity was incremented towards the fusion zone. The HAZ and WZ obtained values of 3.60×10^{-8} and 1.36×10^{-7} respectively. However, for the WZ in its second transient the diffusion rate was minor with a value of 9×10^{-8}.

This type of behavior could indicate that the diffusion rates are low in the base material due to the fact that this area has a greater amount of precipitates, or other defects such as grain boundaries or twins that can reduce the speed with which the hydrogen diffused on the SS type 304 crystal lattice.

This low rate propitiates that hydrogen is easily trapped by these defects, increasing the concentration of hydrogen. However, with the HAZ and WZ there could be a re-distribution or co-precipitation of carbides or nitrides of Ni and Cr, including a dissolution, relying heavily on how

rapidly they precipitate and on the size and distribution of the new generation of these precipitations. If the degree of precipitation is lower, the rapidity with which the hydrogen diffuses increases.

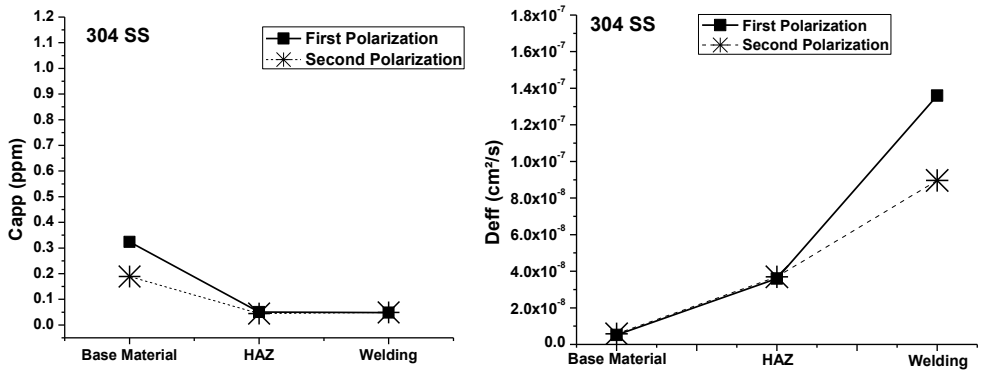

Figure 7. a) hydrogen apparent concentration of 304 steel, b) diffusion rate, in the different welding zones.

3.2.2 SS type 316 hydrogen diffusion.

The hydrogen permeation transients corresponding to the SS type 316 are shown in figure 8. From these transients we could see that the BM, WZ and HAZ transients present a similar performance, achieving the steady state at a normalized time of 0.4. For the second hydrogen transient the time for reaching the steady state of HAZ and WZ was slightly bigger in comparison with the BM with values of 0.7 normalized time. In addition to the fact that the hydrogen permeability values were a little less low than the first hydrogen transient.

The 316 type steel hydrogen transients show a similar behavior to the 304 type steel hydrogen transients, with the only difference that the permeability lows were smaller.

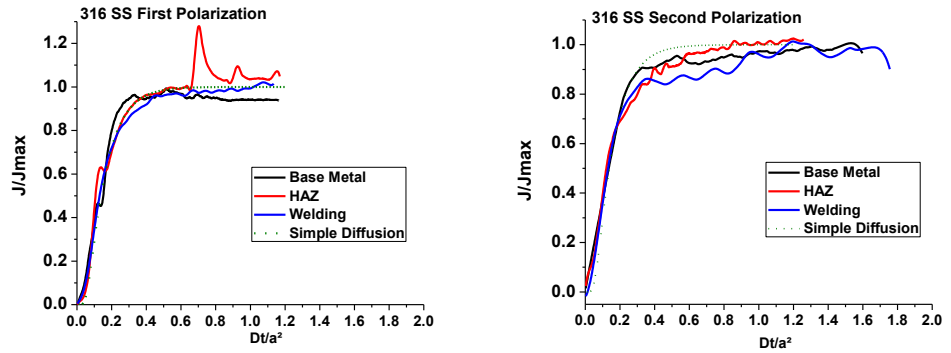

Figure 8. Permeability curves of 316 steel, a) first polarization, b) second polarization.

From the SS type 316 hydrogen permeation first and second transients were obtained from the apparent concentration and hydrogen diffusion rate, see figure 9a and b. The graphs of figure 9 indicate that the BM has the most apparent hydrogen concentration1.1 and 0.3 ppm for the first and second hydrogen transient respectively. The HAZ and WZ show values near 0.05 ppm at the two

transients much lower than the BM, being this behavior exact to the type 304 SS. The BM had a diffusion coefficient of $8.37x10^{-10}$ cm²/s, for both transients this value was identical. The diffusion rate was incremented towards the fusion zone The HAZ and WZ throw values of 4.43×10^{-8} and 1.63×10^{-7} respectively.

However, for the WZ second transient, the diffusion rate was lower with a value of $1.2x10^{-7}$.

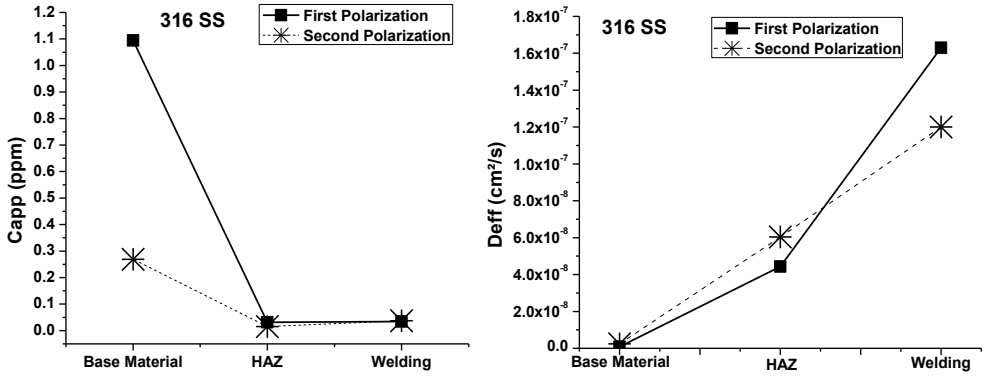

Figure 9. a) hydrogen apparent concentration of 316 steel, b) diffusion rate, in the different welding zones.

4. GENERAL DISCUSSION

To reach hydrogen society goal global technical problems like developing materials capable to resist HE. A lack of detailed studies over The influence of hydrogen on metal remains and the essential Hydrogen-induced Embrittlement mechanism(s) and related phase changes are far from been accomplished. The following discussion and anterior results are an attempt to close the gap for the crucial need for undeveloped, data on the HE mechanisms of candidate materials for hydrogen environments service

From the transients results data we can say that SS type 316 exhibit higher hydrogen concentrations, and somewhat less hydrogen diffusion rates than SS type 304. So the trapping/accumulation of hydrogen at the interfaces between matrix and precipitates could have affected the type 316 BM in a big way indicating that precipitation occurs in this steel, mostly of the chi phase acting as irreversible traps by its Mo content. When cooling the 316 type plates from their hot rolling temperature, it was possible that enough time elapsed to form the chi phase, as it has already been seen the chi phase can form well before the sigma phase. Unfortunately, this second phase is naturally fragile and the addition of hydrogen could make the steel more susceptible to HE.

For steel type 304 the hydrogen concentration between matrix- precipitates- grain boundary interphases could be because of the presence of $Cr_{23}C_6$, that act as u irreversible traps in this steel, as it had already been stated that this carbide can be formed in this austenitic steel type l. Hydrogen trapping among second phase particles and the matrix at interfaces had also been assumed by other

researchers [27-28] as the key cause for HE in austenitic stainless steels. Steel type 304 by its lower hydrogen rates could delay the transport of hydrogen to defects/precipitates/crack tips and the interactions between hydrogen and dislocations more efficiently [29-32]. Thus, impeding HE by matrix-precipitates interphase hydrogen accumulation in the BM.

The higher hydrogen content in type 316 BM could be more susceptible of being brittle by the HELP (Hydrogen Embrittlement Localized Plasticity) mechanism. Gavriljuk et al. [33] propose that the enhancement of the metallic status of the interatomic austenitic SSs bonds by hydrogen atoms, may lead to HELP mechanism, since the metallic character of interatomic bonds rises plasticity and toughness by increased dislocation mobility. Furthermore, the mechanism for type 316 HE was proposed by Hardie and Zheng [34], whereas they argument that the volume of epsilon martensite is directly proportional to SFE (Stacking Fault Energy) which is in contrast to the typical view of hydrogen lowering the SFE. It was reported that in austenitic SSs epsilon martensite is induced by dislocations stress-splitting of soft orientations [35]. For the SSs the SFE over HE is the generation of Lomer-Cottrell locks associated to the falling of SFE by hydrogen [36]. Otherwise, the hydrogen SFE pull down will alter austenite deformation switching from cross slip to planar slip producing ductility loss [37].

During TIG welding, both SSs reach temperatures capable of tore-dissolve all second phases but when cooling both steels can get different cooling temperatures in different zones (HAZ and WZ), in some cases so rapidly that co-precipitation do not take place, and in others in which the time for cooling leads only partial co-precipitation leaving only few low precipitation dense zones. That's why the WZ and HAZ present much lower similar hydrogen concentrations than their BM counterparts. For the hydrogen diffusion rates, it is clearly seen that less trapping sites lead to higher hydrogen mobility through SSs lattice. For both SSs HAZs, the first transient almost ends up occupying all the available site traps and for the second transient it is expected that all traps (irreversible and reversible) are full and that this hydrogen diffusion rate is for only hydrogen passing through the crystal network.

Finally, these results show (figures 9 and 9) that both SSs BM could be more susceptible to HE by their related mechanisms than in their respective lies HAZ and WZ due to their lower hydrogen trapping zones, mostly second phases and precipitates. Apparently, austenitic steel type 304 is more resistant to HE effects, mainly because this steel could trap less hydrogen and deliver hydrogen out from its lattice rapidly. However austenitic type 316 is still a good candidate for HE applications and for its higher resistance to pitting corrosion, and lower susceptibility to sensitization due to its Mo content.

4. CONLUSIONS

The results lead to the following conclusions:

1. TIG welding develop a very good fusion zone along the thickness of the two SSs under study.

2. From specialized literature sources and strong foundations of austenitic SSs knowledge we can infer the different precipitates and second phases of the steels and the first and second respectively hydrogen transients studied, we can deliberate and discuss their different HE behaviors.

3. Steel type 316 was more susceptible to HE effects mainly by its hydrogen concentration in irreversible traps like the chi phase that is a naturally intermetallic brittle phase and with the presence of hydrogen its embrittlement effects could be magnified.

4. Steel type 304 could be embrittled by the formation of $Cr_{26}C_3$ carbide as irreversible trap but Steel type 304 because of its lower hydrogen rates could delay the transport of hydrogen to defects/precipitates/crack tips and the interactions between hydrogen and dislocations more efficiently. Thus, impeding HE by matrix-precipitates interphase hydrogen accumulation in this BM.

5. Austenitic type 316 still is a good candidate for HE applications and for its higher resistance to pitting corrosion, and lower susceptible to sensitization due to its Mo content.

6. The higher hydrogen content in type 316 BM could be more susceptible of being brittled by the HELP (Hydrogen Embrittlement Localized Plasticity) mechanism.

7. Both SSs BM could be more susceptible to HE by their related mechanisms than in their respective HAZ and WZ.

ACKNOWLEDGEMENTS
Authors want to thank Thanks to Mr. Ivan Puente Lee, Facultad de Quimica, UNAM. Also to UNAM PAPIIT-project IN115616, and CONACyT for M.M financial support.

References

1. D. Peckner and I. M. Bernstein, *Handbook of stainless steels*. McGraw-Hill, New York (1977).
2. A. Veziroglu and R. Macario, *Int. J. Hydrogen Energy*, 36 (2011) 25.
3. C. San Marchi, B. P. Somerday, X. Tang and G. H. Schiroky, *Int. J. Hydrogen Energy*, 33 (2008) 889.
4. Design guidelines for the Selection and use of Stainless Steel, A Designer´s Handbook Series, No, 9014, distributed by Nickel Development 1993, p.33.
5. AISI – American Iron and Steel Institute, URL http://www.steel.org/
6. P. S. Korinko and S. H. Malene, *Practical Fail. Anal.*, 1 (2001) 61.
7. J. O. Nilsson, *J. Mater. Sci. Technol.*, 8 (1992) 685.
8. N. R. Quick and H. H. Johnson, *Metall. Trans. A*, 10 (1979) 67.
9. N. Parvathavarthini, S. Mulki, R. K. Dayal, I. Samajdar, K. V. Mani and B. Raj, *Corros. Sci.*, *51* (2009) 2144.
10. J. J. Neuharth and M. N. Cavalli, *Eng. Fail. Anal.*, 49 (2015) 49.
11. S. M. Teus, V. N. Shivanyuk, B. D. Shanina, & V. G. Gavriljuk, *Phys. Status Solidi A*, *204* (2007) 4249.
12. M. B. Djukic, V. S. Zeravcic, G.M. Bakic, A. Sedmak and B. Rajicic, *Eng. Fail. Anal.*, 58 (2015) 485.
13. M. A. V. Devanathan and Z. Stachurski, The adsorption and diffusion of electrolytic hydrogen in palladium. *Proc. Roy. Soc. Lond. Math. Phys. Sci. A*, 1962, 90.
14. L. Joseph, *Weld World*, 31 (1993) 390.
15. A. P Kyriakongonas, V. J.Papazoglou, 3D numerical model of austenitic stainless steel 316L multipass butt welding and comparison with experimental results. Analysis and Design of Marine Structures: including CD-ROM, 2009, vol. 1, p. 371.

16. S. A. David, G. M. Goodwin and D. N. Braski, *Weld. J.*, 58 (1979) 330.
17. S. Kou, Welding Metallurgy, John Wiley and Sons, (2003) Hoboken, NJ, USA.
18. H. K. D. H. Bhadeshia and R. Honeycombe, *Steels Microstructure and Properties* (Butterworth-Heinemann, 2006).
19. I. Calliari, M. Zanesco and E. Ramous, *J. Mater. Sci.*, 41 (2006) 7643.
20. B. Beck, J. O. Bockris, J. McBreen and L. Nanis. *Proc. Roy. Soc. Lond. Math. Phys. Sci. A*, 1966, 290.
21. A. W. Thompson and J. A. Brooks, *Metall. Trans. A*, 6 (1975) 1431.
22. B. G. Pound, *Corros. Sci.*, 42 (2000) 1269.
23. A. M. Brass and J. Chêne, *Corros. Sci.*, 48 (2006) 3222.
24. A. W. Thompson and I. M. Bernstein, Effect of Hydrogen on Behavior of Materials (No. CONF-750925). Metallurgical Society of AIME, New York, 1976.
25. H. K. Birnbaum, in: R. Gibala, R.F. Hehemann (Ed.) Hydrogen Related Second Phase Embrittlement of Solids - Hydrogen Embrittlement and Stress Corrosion Cracking, AMS, 1984, 29.
26. M. Dadfarnia, M. L. Martin, A. Nagao, P. Sofronis and I. M. Robertson, *J. Mech. Phys. Solids*, 78 (2015) 511.
27. S. M. Teus, V. N. Shivanyuk, B. D. Shanina and V. G. Gavriljuk. *Phys. Status Solidi A*, 204 (2007) 4249.
28. D. Hardie and W. Zheng, *Mater. Sci. Tech-Lond.*, 10 (1994) 817.
29. S. M. Teus, V. N. Shyvanyuk, & V. G. Gavriljuk, *Mat. Sci. Eng. A-Struct.*, 497 (2008) 290.
30. S. Jani, M. Marek, R. F. Hochman and E. I. A. Meletis, *Metall. Trans. A*, 22 (1991) 1453.
31. M. I. Luppo, A. Hazarabedian and J. Ovejero-Garcia, *Corros. Sci.*, 41 (1999) 87.